Arch. Metall. Mater. **67** (2022), 2, 555-561

DOI: https://doi.org/10.24425/amm.2022.137790

A. COTAI[1,2], S. MIRAGLIA[2], B.V. NEAMȚU[1], T.F. MARINCA[1], H.F. CHICINAȘ[1,3], O. ISNARD[2], I. CHICINAȘ[1*]

A COMPARATIVE STUDY OF NANOCRYSTALLINE $Fe_{38.5}Co_{38.5}Nb_7P_{15}Cu_1$ ALLOYS OBTAINED BY MECHANICAL ALLOYING AND RAPID QUENCHING

This paper presents a comparative study of the preparation and characterisation of $Fe_{38.5}Co_{38.5}Nb_7P_{15}Cu_1$ alloy produced by mechanical alloying (MA) and rapid quenching (RQ) method. In order to obtain the starting mixture (SS) in the present study, we opted for the replacement of elemental Nb and P powders with ferroalloy powders of niobium and phosphorus. Benzene was used as a control agent of the process (PCA) for wet MA. The samples obtained (powders and ribbons) were characterised by X-ray diffraction (XRD), differential scanning calorimetry (DSC), scanning electron microscopy (SEM), X-ray microanalysis (EDX), magnetic measurements M(H) and thermomagnetic measurements M(T). After 40 h of wet MA, the alloy was partially amorphous, and the ribbons obtained by RQ do not show an amorphous state. Also, the magnetic measurements show the influence of the method used on the magnetic properties.

Keywords: mechanical alloying; melt-spinning; ribbons; magnetisation; ferroalloys

1. Introduction

An amorphous and nanocrystalline alloy is usually described as a dual-phase material consisting of an amorphous metallic phase and nano-sized crystals. Amorphous and nanocrystalline alloys have unique properties, such as outstanding magnetic properties, extraordinary wear/corrosion resistance and superior hardness and strength, improved thermal stability and ductility, properties that are difficult to obtain from amorphous or nanocrystalline alloys separately [1]. Amorphous and nanocrystalline alloys have emerged as a strategy for obtaining a single alloy that combines their best properties. These alloys have good physical, chemical, mechanical and magnetic properties [2-4].

The most important classes of nanocrystalline soft magnetic alloys are FeSiBCuNb alloys, named FINEMET [5], based on FeMBCu, where M = Zr, Nb, Hf etc. alloys, known as NANOPERM [6], and more recently HITPERM, based on FeCoMBCu [7]. The amorphous and nanocrystalline alloys based on iron and cobalt (HITPERM) are known as soft magnetic materials, and their soft magnetic properties persist to $\alpha \rightarrow \gamma$ phase transformation at 980°C. The excellent properties of soft magnetic material in this class of alloys is due to the formation of the α-FeCo phase during the crystallisation process [7,8]. Co addition in HITPERM alloys enhances the Curie temperature of nanocrystalline and amorphous residual phase, and hence, the good exchange coupling between the nanograins is maintained at much higher temperatures as compared to Fe-based alloys (FINEMET and NANOPERM) [9].

The extrinsic property of interest is the magnetic permeability μ(H), which is determined by chemistry, crystal structure, microstructure and morphology [7]. The most known nanocrystalline soft magnetic alloys include in composition metalloids like boron [9], responsible for the glass-former ability and preventing crystallisation. Also, boron increases the thermal stability of the alloy. However, in addition to all the advantages, boron is a relatively expensive element. Therefore, alloys in which boron is substituted to another metalloid would be highly economical. In this paper, we will replace the metalloid boron with phosphorus, and in addition, we will replace the elemental powders with ferroalloys of phosphorus and niobium, which will considerably reduce the production cost of the alloy [10,11].

Amorphous soft magnetic materials can be obtained in several ways: rapid quenching, mechanical alloying, gas atomisation, vapour deposition, etc. The most utilised techniques

[1] TECHNICAL UNIVERSITY OF CLUJ-NAPOCA, MATERIALS SCIENCE AND ENGINEERING DEPARTMENT, 103-105 MUNCII AVE., 400641 CLUJ-NAPOCA, ROMANIA
[2] INSTITUT NÉEL, CNRS / UNIVERSITÉ GRENOBLE ALPES, 25 RUE DES MARTYRS, BP166, 38042 GRENOBLE, CÉDEX 9, FRANCE
[3] GUHRING ROMANIA, CONSTRUCTURILOR STREET 30, APAHIDA 407035, ROMANIA

* Corresponding author: ionel.chicinas@stm.utcluj.ro

are rapid quenching (RQ) in the form of ribbons [12] and mechanosynthesis in powder form [13]. During MA, due to the increase of the powder temperature on the one hand, and a large number of structural defects induced, on the other hand, interatomic diffusion is favoured and finally, the alloy formation. A quantity of process control agent (PCA) was added to reduce the frequency of cold welding and prevent the agglomeration of the particles [14].

In this work, we have investigated the (Fe, Co)-M-B-Cu, where we substituted P for metalloid B and choosing M = Nb; the alloy is produced by either wet mechanical alloying or rapid solidification processing. Structural and morphological properties, as well as magnetic properties of Fe38.5Co38.5Nb7P15Cu1 alloys, were measured and compared according to the preparation method.

2. Materials and methods

Starting materials were iron powder (Höganäs NC 100.24), cobalt powder (99.99%), copper powder (99.78%) and ferroalloys powders of niobium (58.78wt.% Nb, 41.22wt.% Fe) and phosphorus (24.1wt.% P, 75.9 wt.% Fe). They were mixed in a Turbula type apparatus for 20 minutes to obtain a better homogenisation of the starting mixture (SS) with the composition $Fe_{38.5}Co_{38.5}Nb_7P_{15}Cu_1$ (at.%). The starting mixture was subjected to mechanical alloying (MA) and rapid cooling (RQ). The MA experiments were processed in a high energy ball mill (Fritsch Pulverisette 6), with steel balls (14.6 mm) and tempered steel milling vials (500 mL). The milling experiments were performed at a rotation speed of 350 rpm, high purity argon atmosphere and a 16:1 ball-to-powder mass (BPR) ratio. The process control agent added in this case was benzene (C_6H_6), and the samples were milled up to 40 h. In this mechanical alloying experiment, 1 mL of C_6H_6 was added in the milling vial after 2 h of milling and after each sampling procedure. Benzene was used as PCA in order to avoid powder agglomeration and to minimise the cold welding between particles during MA. For investigation, samples were taken at milling intervals of 2, 5, 10, 20, 30, and 40 hours.

In the case of RQ experiments, the starting mixture was melted in an arc melter to produce $Fe_{38.5}Co_{38.5}Nb_7P_{15}Cu_1$ alloy ingots. For these experiments, the same composition of SS was used as in the case of MA. After that, the ingots are placed in a quartz tube with a slit nozzle and subjected to induction melting in an argon atmosphere. The molten alloy is pushed down the quartz crucible nozzle by pressurised argon gas (250 mbar overpressure). The liquid was then ejected on the polished surface of a copper wheel rotating at a linear speed of 20 m/s.

The melt comes in contact with the water-cooled copper wheel, and the alloy ribbons are formed. The rapid cooling experiments were performed using modified commercial equipment (Buehler Melt Spinner). The RQ experiments respected the following parameters: the wheel was made of copper, tangential wheel speed was 52 m/s, the crucible was made of quartz, melting of the sample was done by induction, the distance between nozzle and rotating wheel was 200 μm, and atmosphere – high purity argon. The ribbons were prepared by single roller melt spinning.

The structural evolution of the powders was investigated by X-ray diffraction (XRD). The XRD patterns for powders were recorded using cobalt K_α radiations with the wavelength of λ = 1.79026 Å, in the angular range 2θ = 20-110°. The equipment used was an Inel Equinox 3000 X-ray powder diffractometer, working in reflection mode. And respectively, the XRD for ribbons was recorded using Cu-K_α radiations with the wavelength of λ = 1.54185 Å (diffractometer Bruker D8 Endeavor). The morphology and the chemical homogeneity of the powders were characterised by a Sigma Gemini Zeiss scanning electron microscope (SEM) equipped with an energy dispersive spectrometer (EDX). The thermal stability of the samples was investigated by differential scanning calorimetry (DSC) using a Setaram Labsys installation. The analysed temperature range was 20-1000°C, with a heating and cooling rate of 10°C/min. DSC experiments used high purity alumina as a reference and under high purity Ar atmosphere.

Magnetisation isotherms M(H) were measured using a superconductive coil magnetometer, which works on the principle of axial extraction of the sample from the magnetic field. The measurements were performed at 300 K in an applied magnetic field up to 8 T.

3. Results and discussions

The X-ray diffraction patterns (XRD) plotted in Fig. 1 has been measured at room temperature for $Fe_{38.5}Co_{38.5}Nb_7P_{15}Cu_1$ powders milled up to 60 hours using benzene as PCA. The characteristic peaks of the α-Fe, FeNb, FeP, fcc Co and hcp Co structures are revealed in the XRD pattern of the unmilled powders (SS). The XRD investigation of the elemental Co powder used for starting samples reveals the coexistence of face-centred-cubic (fcc) and hexagonal close-packed (hcp) allotropes [15]. In Fig. 1 it can be seen that, upon increasing the milling time, there are a decrease in the intensity and a broadening of the Bragg peaks. This is due to the second-order internal stresses induced during the MA process and decreased crystallites size by milling. Also, the displacement of the peaks to smaller angles results from first-order internal stresses induced by MA [16]. By increasing the milling time, some of the characteristic peaks are disappearing, suggesting the progressive introduction of the elements in the Fe lattice. Smearing and broadening of the peaks mean loss of long-range ordering. After 5 h of milling, the Bragg reflections of hexagonal Co are disappearing.

The several maxima shown in the diffractogram suggest that the complete dissolution of the elements in solid solution based on Fe and Co did not occur. After 30 h of wet milling with benzene, the material is almost in an amorphous state. By continuing to mill for up to 40 and 60 hours, a crystallisation induced mechanically occurs, and the most intense Bragg maxima of Fe_3P compound is clearly visible. The long-range atomic ordering is confirmed on the diffractogram, which does

not characterise an amorphous alloy [9]. In this case, complete amorphisation of the alloy is not observed even after 60 h of milling. This behaviour suggests that total replacement of the amount of B with P in $Fe_{38.5}Co_{38.5}Nb_7B_{15}Cu_1$ alloy does not lead to a full amorphisation of the powder, as in the case of the alloy containing B only processed in similar milling conditions [17].

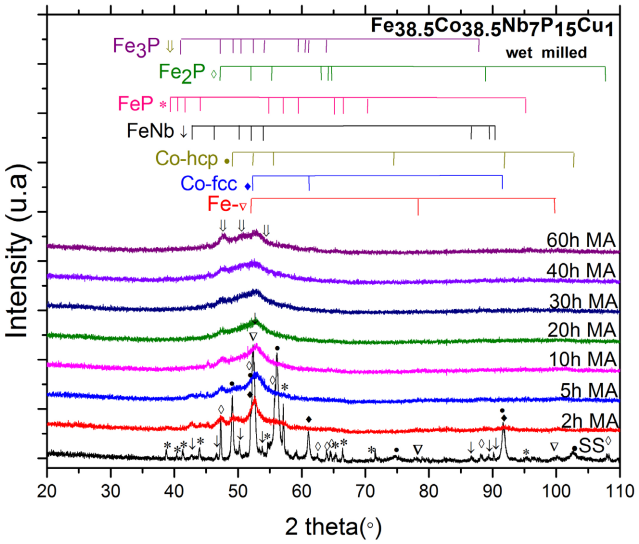

Fig. 1. Room temperature X-ray diffraction patterns of the starting sample (noted SS) and of the $Fe_{38.5}Co_{38.5}Nb_7P_{15}Cu_1$ samples wet milled for the indicated milling duration up to 60 hours

However, the obtained powder consists of an amorphous matrix (the main phase) that embed the nanocrystalline phase of Fe_3P.

The general aspect of $Fe_{38.5}Co_{38.5}Nb_7P_{15}Cu_1$ ribbons is presented in Fig. 2, showing that the ribbons do not have a continuous and well-defined shape. Long ribbons with this composition have short dimensions and are difficult to obtain using the current experimental conditions of the melt-spinning process. The melt-spun $Fe_{38.5}Co_{38.5}Nb_7P_{15}Cu_1$ ribbons were characterised by X-ray diffraction shown in Fig. 3. As in the case of wet MA experiments, amorphous samples were not obtained.

Fig. 2. The general aspect of the melt-spun $Fe_{38.5}Co_{38.5}Nb_7P_{15}Cu_1$ ribbons

The sharp diffraction peaks (Fig. 3) confirm the crystallinity of the alloy ribbons. For a better analysis of the amorphous state of the ribbons, X-ray diffractions were performed on both sides of the ribbons. Fig. 3 shows the XRD diffractions of the obtained ribbon, Fig. 3(a) shows the diffraction for the face of the ribbon that did not come in contact with the cooling cooper wheel (air side named F1), and Fig. 3(b) – the face of the ribbon which was in contact with the copper wheel (wheel side named F2). The XRD patterns of both faces of the ribbon present several peaks corresponding to FeCo and Fe_4P, Fe_3P and FeP phases. Assigning the peaks to one phase or another was very difficult to achieve due to the weakness of the Bragg peaks on the one hand and the multiphase character of the ribbons on the other hand.

By estimating the integral intensity of the peaks of crystalline phases and the integral intensity of those of the amorphous phase for both sides of the ribbons, it can be mentioned that the F2 face contains a larger amount of amorphous phase. This is given by the more rapid cooling of this face, which is in contact with the copper spinning wheel, compared to face F1. The partial crystallisation of the ribbon, prooved by XRD investigation, is well correlated

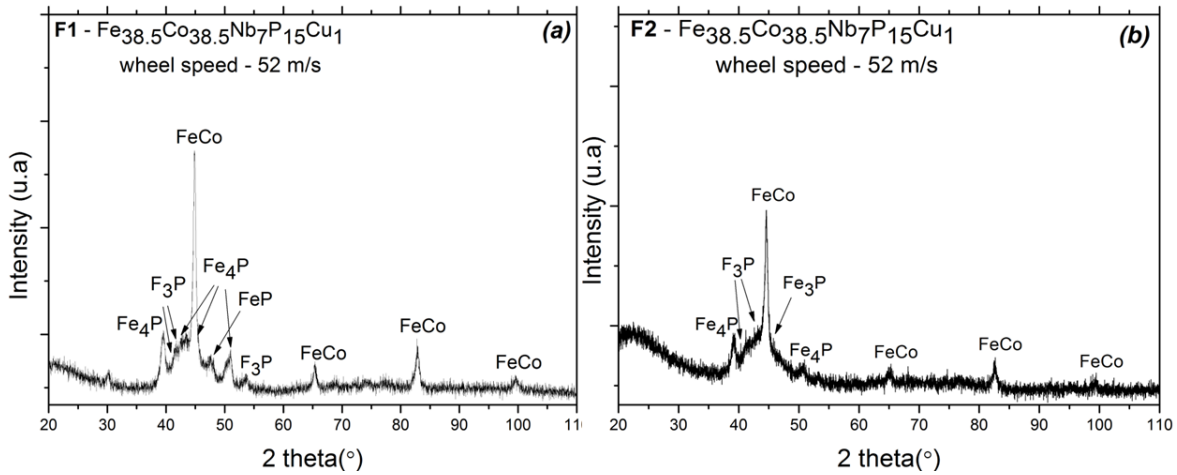

Fig. 3. X-ray diffraction patterns of the $Fe_{38.5}Co_{38.5}Nb_7P_{15}Cu_1$ ribbons prepared by rapid quenching, (a) – the face (F1) of the ribbon that did not come in contact with the cooling disk and (b) – the face (F2) of the ribbon that came in contact with the copper wheel (λ = 1.54185 Å)

with the macroscopic aspects of the ribbons. It is known that when an amorphous ribbon is subjected to a heat treatment that induces its crystallisation, the crystallised ribbon become very brittle. This may be explained why the here obtained ribbons were obtained as short ribbons and not continuous, long ribbons.

The morphological evolution of the $Fe_{38.5}Co_{38.5}Nb_7P_{15}Cu_1$ powders as a function of milling time is shown in Fig. 4. In the SEM image on the left side, it can be observed that after 5 h of milling, the powder is formed by particles with polyhedral shape. After 40 h of milling, the SEM image on the right side shows a decrease in the average particle size for such a longer milling time, and the particles have a similar irregular shape as in the case of short milling time. The SEM images obtained at 10,000× magnification highlight the polyhedral shape of the particles formed by the agglomeration of micrometric and even nanometric particles.

The EDX studies on the chemical homogeneity of the powders wet-milled up to 40 h are shown in Fig. 5. The uni-

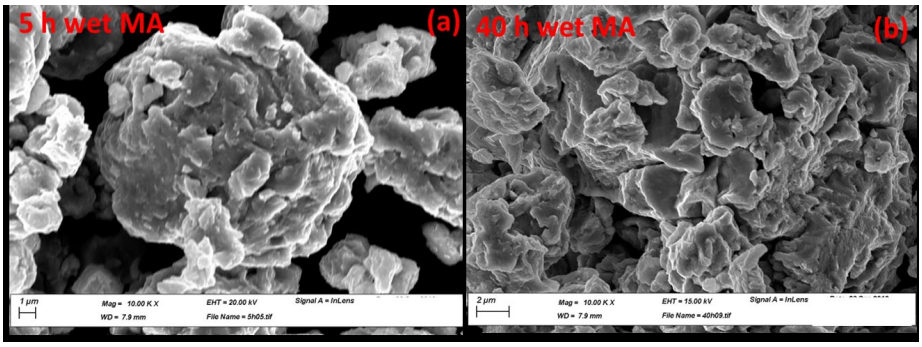

Fig. 4. SEM images of $Fe_{38.5}Co_{38.5}Nb_7P_{15}Cu_1$ powders wet-milled at 10,000× magnification; (a) – 5 h wet-milled and (b) – 40 h wet-milled

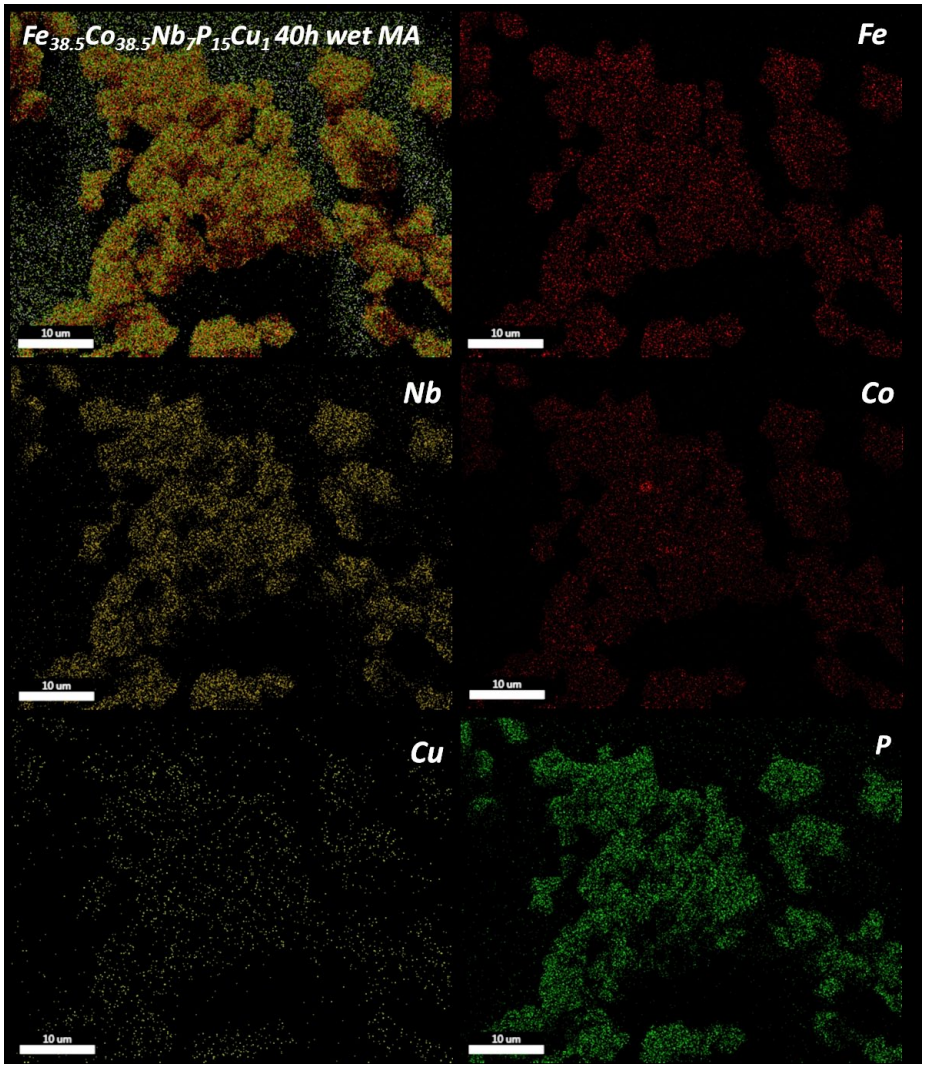

Fig. 5. X-ray microanalysis of powders obtained on the surface of a particle wet milled for 40 h. Distribution maps for P, Nb, Fe, Co and Cu

form distribution of the elements on the powder surface can be observed; however, this is not a confirmation of the formation of the alloy without X-ray investigations.

Fig. 6 shows the DSC curve of $Fe_{38.5}Co_{38.5}Nb_7P_{15}Cu_1$ powder recorded upon heating in the room to 1000°C temperature range. For a better comparison of the events that take place in the alloy during the heating, we also carried out the thermomagnetic analysis. Fig. 8 presents the magnetisation curve recorded versus temperature M(T) up to 1000°C. The Curie temperature of the amorphous phase derived from the M(T) curve is about 270°C. The DSC curve of the sample obtained by wet MA up to 40 h using benzene as PCA consists of a series of exothermic and endothermic events – Fig. 6. The first exothermic maximum can be observed in the temperature range of 130-320°C, and it is attributed to the recovery and structural relaxation of stresses induced in particles by the mechanical alloying process [14]. These transformations are characteristic for the amorphous/ nanocrystalline alloys obtained by MA subjected to annealing, proving that the powder MA for 40 h is partially amorphous [18]. The second event (visible on both curves made on powders) is an exothermic peak centred at about 450°C, and it is attributed to the primary crystallisation of the amorphous phase present in the sample. A Fe-Co solid solution is formed. Increasing the temperature, at about 550°C, can be observed an intense exothermic peak. This second crystallisation phenomenon is also identified on both curves DSC and M(T) of powder. During this crystallisation, it is possible to precipitate the NbC phase.

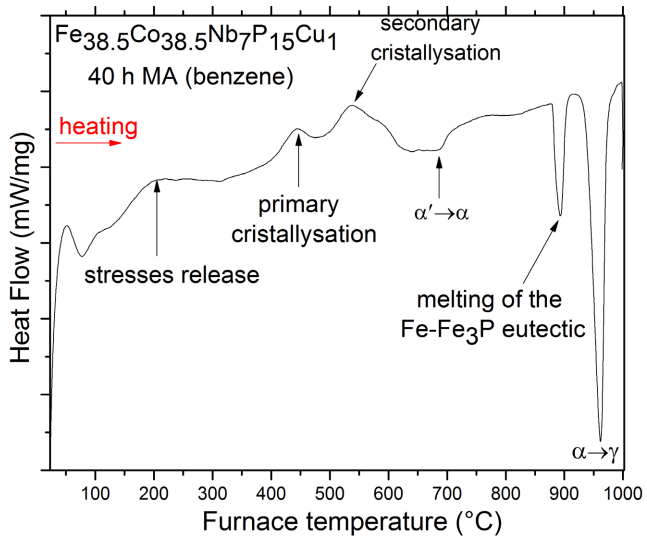

Fig. 6. DSC curve of $Fe_{38.5}Co_{38.5}Nb_7P_{15}Cu_1$ alloys wet-milled 40 hours

Contamination with carbon atoms during wet milling samples and the formation of the NbC phase is plausible considering the affinity of the Nb for C [19]. Carbon atoms result from the decomposition of benzene during the thermomechanical process. Most likely, they are incorporated into the alloy during milling and heating. They favour the formation of niobium carbide [17,20]. The presence of carbon atoms in the alloy is expected to play a significant role both in the amorphisation of the milled powder and in the crystallising phases. After the precipitation of a non-magnetic phase such as NbC (formed by two non-magnetic atoms), the magnetic interactions between ferromagnetic atoms increase, and the magnetisation of the alloy increases, as can be seen on the curve M (T), Fig. 7. The endothermic peak at about 700°C is attributed to the α' → α phase transition. According to the Fe-Co diagram, this phase transition is a transition from an ordered structure to a disordered structure [21]. A pronounced endothermic peak can also be observed at about 880°C, assigned to the melting temperature of the Fe-Fe_3P eutectic. In the Fe-P phase diagram, the Fe-Fe_3P eutectic has a melting temperature of 1076°C [22], but in the mechanically alloyed powders, it is possible to decrease the melting temperature by mechanical activation. Another high-intensity endothermic peak is visible on the DSC curve at about 900°C; this peak was assigned to α → γ (bcc to fcc) phase transition [8]. The soft magnetic properties of $Fe_{38.5}Co_{38.5}Nb_7P_{15}Cu_1$ alloy persist up to the α → γ phase transformation. Indeed, in the thermomagnetic M(T) curve recorded on powders, presented in Fig. 7(a), it can be observed that the powder become paramagnetic after this transformation.

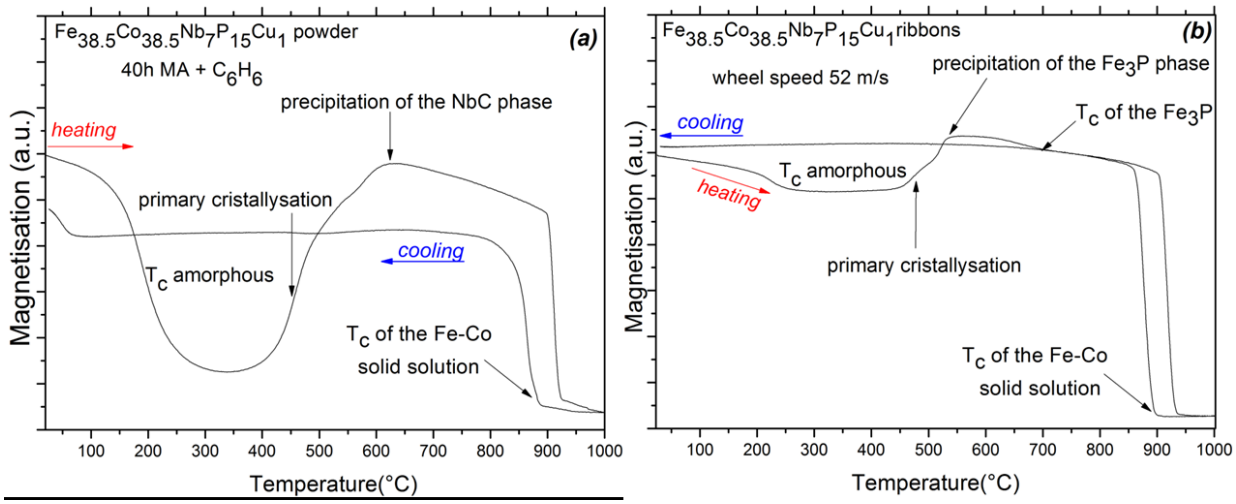

Fig. 7. Thermomagnetic M(T) curves of the $Fe_{38.5}Co_{38.5}Nb_7P_{15}Cu_1$ samples (a) – obtained after 40 h of wet mechanical milling and (b) – ribbons prepared by rapid quenching

In the case of the M(T) curve made on the ribbons obtained by RQ from the same composition, presented in Fig. 7(b), it is also observed the Curie temperature of the amorphous phase around 270°C, followed by an increase of the magnetisation. This is due to the primary crystallisation of the amorphous phase and the formation of a Fe-Co solid solution. At around 700°C it is observed a slight drop in magnetisation, which corresponds to the Curie temperature of Fe_3P compound [23]. This Curie temperature is not observed on the M(T) cooling curve. A possible explanation could be that the P atoms are dissolved in Fe-Co solid solution during heating up to 1000°C. The thermomagnetic curves recorded upon cooling in both cases (powder and ribbon) did not show other magnetic transformations.

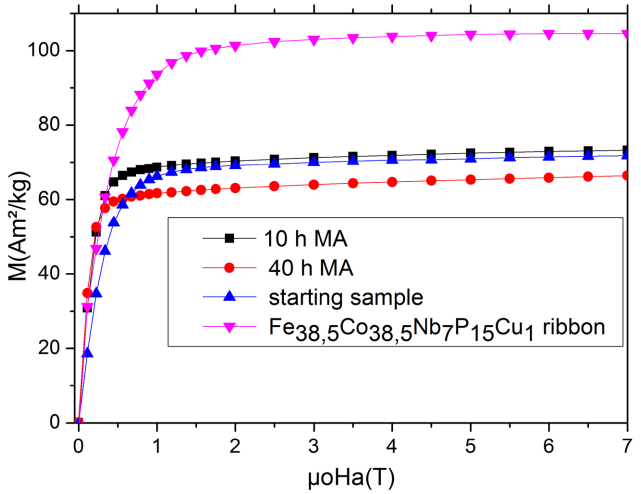

Fig. 8. Evolution of the magnetisation curves, recorded at 300 K, of the $Fe_{38.5}Co_{38.5}Nb_7P_{15}Cu_1$ powder milled up to 40 h and the ribbon's saturation magnetisation with the same composition

The evolution of the 300 K magnetisation curves of the $Fe_{38.5}Co_{38.5}Nb_7P_{15}Cu_1$ powders wet-milled up 40 h and ribbons of the same composition obtained by melt spinning are presented in Fig. 8. For a good comparison, the magnetisation curve for the starting sample is also shown. After 10 h of wet milling, a slight increase in saturation magnetisation can be observed. This small increase of saturation magnetisation can be attributed to contamination of the powder with Fe from the milling balls and vial, both made of steel [24]. By increasing the milling time to 40 h, a decrease of saturation magnetisation can be noticed. The decrease of the saturation magnetisation is the result of the following phenomena: (i) introduction of non-ferromagnetic atoms (Nb, Cu, P) in the structure of the FeCo-based solid solution with the increase of the milling time, resulting in a long-range order degradation of magnetic atoms [25,26]; (ii) introduction of a large number of structural defects during mechanical alloying, crystallites size reduction and the progressive amorphisation. All these aspects previously mentioned can increase the distances between the magnetic atoms and can lead to the diminution of the magnetic interaction; thus, the magnetisation of the powders decreases [27]; (iii) the presence of a PCA agent (benzene) during the MA process leads to the contamination of the powders with non-ferromagnetic atoms resulting from the decomposition of the benzene. The presence of a non-magnetic substance, such as benzene, on the surface of the particles, leads to a decrease in the number of magnetic atoms per unit mass; thus, a decrease of saturation magnetisation was identified. With increasing milling time, the specific surface increases and also, a more pronounced diminution of the saturation magnetisation can be expected [28].

If we compare the saturation magnetisation of $Fe_{38.5}Co_{38.5}Nb_7P_{15}Cu_1$ powders obtained by wet MA with that of the ribbons, we can see a difference of about 40%, much larger magnetisation being obtained for the ribbons. The large difference can be explained by several aspects: (i) the difference of the degree of crystallinity, (ii) the presence/absence of benzene in the composition during the annealing, (iii) structural defects and (iv) the stress release [29].

4. Conclusions

Preparation of $Fe_{38.5}Co_{38.5}Nb_7P_{15}Cu_1$ at.% in the fully amorphous state via wet mechanical alloying, using benzene as a process control agent (PCA), was not possible under the conditions presented in this study. Also, in the case of rapid quenching, we did not obtain amorphous ribbons. The SEM+EDX studies highlighted the chemical homogeneity and polyhedral shape of the particles formed by the agglomeration of micrometric and even nanometric particles. The wet MA powder for up to 60 hours was partially amorphous, proven by the DSC curve, which shows a series of exothermic and endothermic events characteristic of the amorphous structure. Structural transformations were reported from the DSC curves: the primary crystallisation of the amorphous phase, the crystallisation of NbC phase, α'-Fe(Co) → α-Fe(Co) order-disorder transition, melting of the Fe-Fe_3P eutectic and α → γ (bcc to fcc) phase transition. The thermomagnetic heating curves showed two magnetic phases on the 40 h milled powders (amorphous phase and Fe-Co based solid solution) and three magnetic phases in the ribbons (amorphous phase, Fe_3P and Fe-Co based solid solution). The larger saturation magnetisation (with 40%) of the ribbons compared with the one of powders with the same composition is assigned to the absence of benzene in the ribbons, stress release, different degree of crystallinity and amount of the structural defects. In conclusion, the total P for B metalloid replacement in the composition (Fe, Co)-M-B-Cu (HITPERM) does not lead to the total amorphisation of the alloy neither by the MA method nor by rapid quenching.

Acknowledgement

This paper was supported by the Project "Entrepreneurial competencies and excellence research in doctoral and postdoctoral programs – ANTREDOC", project co-funded by the European Social Fund. Also, these results were partially supported by the Romanian Ministry of Research and Innovation by project 21 PFE in the frame of the programme PDI-PFE-CDI 2018,

and by the European Development Fund and the Romanian Government through the Competitiveness Operational Programme 2014-2020, project ID P 34 466, MySMIS code 121349, contract no. 5/05.06.2018

REFERENCES

[1] F. C. Li, T. Liu, J.Y. Zhang, S. Shuang, Q. Wang, A.D. Wang, J.G.Wang., Mater. Today Adv. **4**, 100027 (2019).

[2] C. Suryanarayana, C.C. Koch, Hyperfine Interact. **130** (1-4), 5-44 (2000).

[3] M.L. Trudeau, J.Y. Ying, Nanostructured Mater. **7** (1-2), 245-258 (1996).

[4] K.S. Kumar, H. Van Swygenhoven, S. Suresh, Acta Mater. **51** (19), 5743-5774 (2003).

[5] Y. Yoshizawa, S. Oguma, K. Yamauchi, J. Appl. Phys. **64**, 6044-6046 (1988).

[6] K. Suzuki, A. Makino, N. Kataoka, A. Inoue, T. Masumoto, Mater. Trans. JIM **32** (1), 93–102 (1991).

[7] M.A. Willard et al., J. Appl. Phys. **84** (12), 6773-6777 (1998).

[8] J.E. May, M.F. De Oliveira, S.E. Kuri, Mater. Sci. Eng. **361**, 179-184 (2003).

[9] M.E. McHenry, M.A. Willard, D.E. Laughlin. **44** (4), (1999).

[10] M.M. Gasik, Introduction, Twelfth Ed. Elsevier, (2013).

[11] K. Tanaka, Energy Policy **36** (8), 2887-2902 (2008).

[12] C. Suryanarayana A. Inoue, Bulk Metallic Glasses, CRC Press, New York 2011.

[13] C.C. Koch, Mater. Sci. Eng. A **244** (1), p. 39-48, 1998.

[14] B.V. Neamţu, O. Isnard, I. Chicinaş, C. Vagner, N. Jumate, P. Plaindoux, Mater. Chem. Phys. **125** (3), 364-369 (2011).

[15] J.Y. Huang, Y.K. Wu, H.Q. Ye, Appl. Phys. Lett. **44** (3), 308 (1995).

[16] B.V. Neamţu, H.F. Chicinaş, T.F. Marinca, O. Isnard, I. Chicinaş, J. Alloys Compd. **673**, 80-85(2016).

[17] A. Cotai, B.V. Neamţu, F. Popa, T.F. Marinca, O. Isnard, I. Chicinaş, J. Alloys Compd. **880**, 160497 (2021).

[18] S. Souilah, S. Alleg, C. Djebbari, R. Bensalem, J.J. Suñol, Mater. Chem. Phys. **132** (2-3), 766-772 (2012).

[19] Y. Kato, M. Ito, Y. Kato, O. Furukimi, Mater. Trans. **51** (9), 1531-1535 (2010).

[20] B.V. Neamţu, H.F. Chicinaş, T.F. Marinca, O. Isnard, O. Pană, I. Chicinaş, Mater. Chem. Phys. **183**, 83-92(2016).

[21] C. Turk, H. Leitner, G. Kellezi, H. Clemens, W.M. Gan, P. Staron, S. Primig., Mater. Sci. Eng. A **662**, 511-518 (2016).

[22] A. I. Zaitsev, Z. V. Dobrokhotova, A. D. Litvina ,B. M. Mogutnov, J. Chem. Soc. Faraday Trans. **91**, 703-712.

[23] N.S. Kazama, T. Masumoto, M. Mitera, J. Magn. Magn. Mater. **15-18**, 1331-1335 (1980).

[24] C. Suryanarayana, Prog. Mater. Sci. **46** (1-2), 1-184 (2001).

[25] O. Isnard, D. Fruchart, J. Alloys Compd. **205** (1-2), 1-15 (1994).

[26] C. Chacon, O. Isnard, J. Appl. Phys. **89** (1), 71-75 (2001).

[27] A.H. Taghvaei et al., Mater. Chem. Phys. **134** (2-3),1214-1224 (2012).

[28] A. Nouri a, C. Wen, Crit. Rev. Solid State Mater. Sci. **39** (2), 81-108 (2014).

[29] B.V. Neamţu, T.F. Marinca, I. Chicinaş, O. Isnard, J. Alloys Compd. **626**, 49-55 (2015).